ACCOUNTS
of chemical research

# Two-Dimensional Electronic Spectroscopy of Molecular Excitons

FRANZ MILOTA,[†] JAROSLAW SPERLING,[†,§] ALEXANDRA NEMETH,[†]
TOMÁŠ MANČAL,[‡] AND HARALD F. KAUFFMANN[*,†,⊥]

[†]*Department of Physical Chemistry, University of Vienna, 1090 Vienna, Austria,* [‡]*Faculty of Mathematics and Physics, Charles University in Prague, 121 16 Prague 2, Czech Republic,* [⊥]*Ultrafast Dynamics Group, Technical University of Vienna, 1040 Vienna, Austria*

RECEIVED ON DECEMBER 30, 2008

Downloaded by RENMIN UNIV OF CHINA on October 2, 2009 | http://pubs.acs.org
Publication Date (Web): August 12, 2009 | doi: 10.1021/ar800282e

## CONSPECTUS

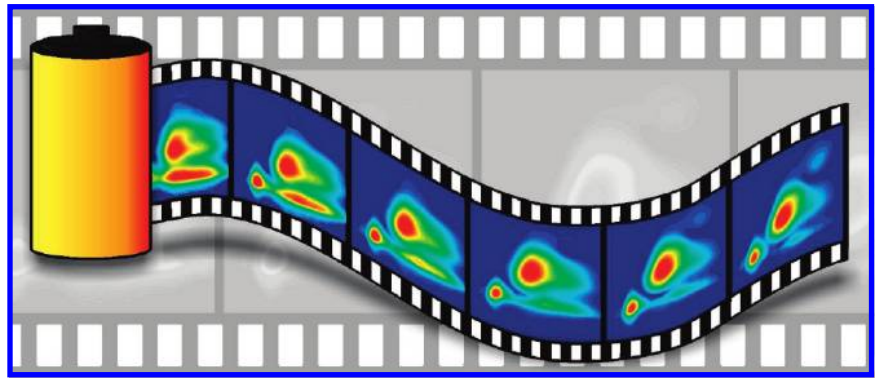

Understanding of the nuclear and electronic structure and dynamics of molecular systems has advanced considerably through probing the nonlinear response of molecules to sequences of pulsed electromagnetic fields. The ability to control various degrees of freedom of the excitation pulses—such as duration, sequence, frequency, polarization, and shape—has led to a variety of time-resolved spectroscopic methods. The various techniques that researchers use are commonly classified by their dimensionality, which refers to the number of independently variable time delays between the pulsed fields that induce the signal. Though pico- and femtosecond time-resolved spectroscopies of electronic transitions have come of age, only recently have researchers been able to perform two-dimensional electronic spectroscopy (2D-ES) in the visible frequency regime and correlate transition frequencies that evolve in different time intervals. The two-dimensional correlation plots and their temporal evolution allow one to access spectral information that is not exposed directly in other one-dimensional nonlinear methods.

In this Account, we summarize our studies of a series of increasingly complex molecular chromophores. We examine noninteracting dye molecules, a monomer−dimer equilibrium of a prototypical dye molecule, and finally a supramolecular assembly of electronically coupled absorbers. By tracing vibronic signal modulations, differentiating line-broadening mechanisms, analyzing distinctly different relaxation dynamics, determining electronic coupling strengths, and directly following excitation energy transfer pathways, we illustrate how two-dimensional electronic spectroscopy can image physical phenomena that underlie the optical response of a particular system.

Although 2D-ES is far from being a "turn-key" method, we expect that experimental progress and potential commercialization of instrumentation will make 2D-ES accessible to a much broader scientific audience, analogous to the development of multidimensional NMR and 2D-IR.

## Introduction

Multidimensional Fourier transform nuclear magnetic resonance (NMR)[1,2] spectroscopy of spin transitions has revolutionized structural biology. Inspired by the huge success of two-dimensional NMR, analogous spectroscopic concepts also have


Published on the Web 08/12/2009 www.pubs.acs.org/acr
10.1021/ar800282e CCC: $71.50 © 2009 American Chemical Society

Downloaded by RENMIN UNIV OF CHINA on October 2, 2009 | http://pubs.acs.org
Publication Date (Web): August 12, 2009 | doi: 10.1021/ar800282e

been realized in the infrared (IR) region of the electromagnetic spectrum.[3−6] Mainly because of the necessity of constant phase relations between excitation pulses, the implementation of two-dimensional electronic spectroscopy (2D-ES) in the visible was stalled and lagged the IR counterparts by several years. Meanwhile, after the first reports of 2D-ES experiments on dye molecules in the near-IR,[7,8] the range of investigated systems is being extended continuously to samples like covalently linked dimers,[9] photosynthetic complexes,[10−12] quantum wells,[13−15] or atomic vapors.[16,17]

The principle of 2D-ES is based on the correlation of electronic coherences, that are generated by a sequence of three femtosecond laser pulses and evolve during two time intervals. The first laser pulse (with wavevector $\mathbf{k}_1$) creates a coherence between the ground and the first excited state, which evolves for a time $t_1$. The second pulse $\mathbf{k}_2$ converts the coherence into a population (or a vibrational wavepacket), either in the ground or the excited electronic state. After a time $t_2$, again electronic coherences are created by the third pulse $\mathbf{k}_3$, which either once more couples the ground and first excited state or the first and second excited states. The induced third-order polarization $P^{(3)}(t_1,t_2,t_3)$ finally radiates the signal field $E_S^{(3)}(t_1,t_2,t_3)$ in a direction dictated by phase-matching conditions. Detection of the signal by spectral interferometry, that is, by mixing with a local oscillator (LO) pulse, permits a complete characterization of the field's amplitude and phase.[7,18] To attain the desired 2D frequency−frequency correlation spectrum, $E_S^{(3)}(\omega_1,t_2,\omega_3)$, two Fourier transforms (FT) have to be performed, one of which ($t_3 \rightarrow \omega_3$) is inherent to the detection scheme.[19] The FT $t_1 \rightarrow \omega_1$ is obtained by scanning the temporal separation of the first and second excitation pulse ($t_1$) over a predefined range and a subsequent FT of the signals with respect to $t_1$.

The described procedure, which might sound rather tedious compared with other third-order nonlinear techniques, bears a number of unique advantages. Obviously, spreading the information content into two frequency dimensions facilitates the interpretation of congested spectra. Apart from this fact, it is essential to realize that the method characterizes both the real (absorptive) and imaginary (dispersive) parts of the complex nonlinear signal, so in fact, any other third-order experiment is contained in the 2D spectrum.[20] While the spectral resolution of a 2D experiment is practically only limited by the maximal delay between the first two interactions, its temporal resolution is given by the accuracy in timing the interaction sequence, that is, by the pulse durations. Two-dimensional electronic spectroscopy thus overcomes the trade-off between time and frequency resolution that is imposed by the time−bandwidth product of the excitation pulses to other techniques.

This Account, in which we condense our contributions to the field of 2D-ES, is devoted to illustrate the above arguments. We present experimental and theoretical studies of molecular systems that can be differentiated by their structural complexity and whose optical response consequently is determined by different physical phenomena. For the simplest possible case of an electronic two-level absorber, we trace the motion of a low-frequency vibrational wavepacket that is reflected in the beating of the 2D line shapes.[21] By simultaneously monitoring monomers and van-der-Waals bound dimers in a single experiment, we then illustrate how 2D line shapes are affected by exciton delocalization induced by electronic intermolecular couplings.[22] Finally, we find electronic couplings to dominate the optical response of a supramolecular aggregate, for which we characterize the motion of excitons that relax across a multiband spectrum.[23,24]

## Experimental Technique

Excitation in the visible is accomplished by a noncollinear optical parametric amplifier (NOPA), which is pumped at a repetition rate of 200 kHz.[25] Our system delivers sub-20 fs pulses tunable from 500 to 700 nm with pulse energies exceeding 200 nJ. To compensate dispersive elements of the setup and the NOPA, we apply a combination of Brewster-angled chirped mirrors and a conventional prism compressor.[26] For full characterization of the pulses and to ensure their shortest possible duration at the position of the sample, we apply spectral interferometry (ZAP-SPIDER).[27] Based upon the work of Miller and co-workers and Fleming and co-workers,[10,28] we have implemented a passively phase-stabilized, diffractive optics based setup. Figure 1 shows the layout of the 2D-ES experiment, the definition of delay times (left inset), and the detection scheme (right inset).[29]

Two-dimensional spectra are acquired by scanning delay $t_1$ (separating the first two interactions of the sample with the pulse sequence) symmetrically around $t = 0$ while keeping delay $t_2$ between the second and third interaction constant. This scanning protocol collects nonrephasing contributions in the wavevector architecture $\mathbf{k}_s = +\mathbf{k}_1 - \mathbf{k}_2 + \mathbf{k}_3$ for negative values of $t_1$ and rephasing contributions in the direction $\mathbf{k}_s = -\mathbf{k}_1 + \mathbf{k}_2 + \mathbf{k}_3$ for positive $t_1$ values. The Fourier transform of this data into $\omega_1$ gives purely absorptive real parts and purely dispersive imaginary parts of the 2D spectrum by equally weighting the rephasing and nonrephasing contributions.[30] For all samples, the $t_1$ delays are scanned with a resolution of 0.65 fs, which is above the Nyquist frequency dictated by elec-

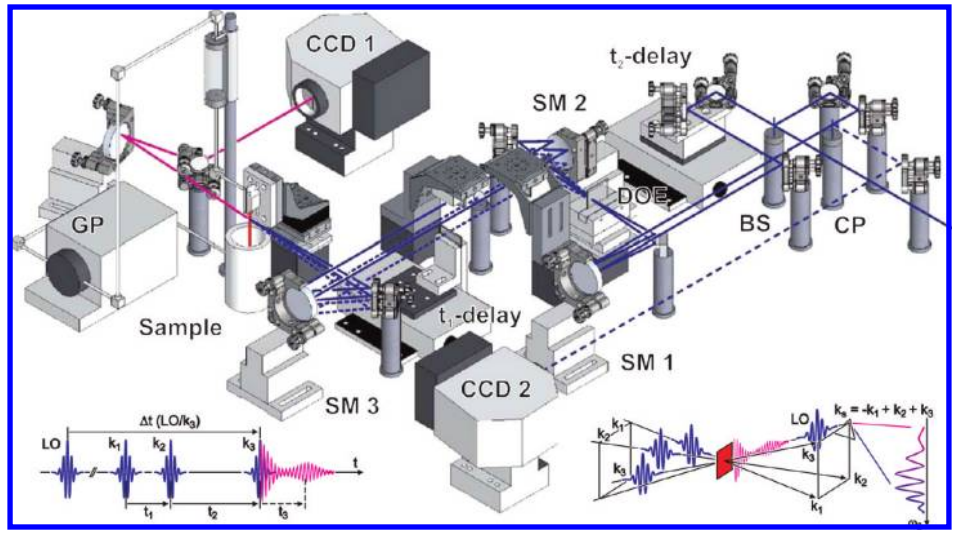


**FIGURE 1.** Experimental setup with pump−probe extension: BS = beam splitter; CP = compensation plate; DOE = diffractive optical element; SM = spherical mirror; GP = gear pump; CCD = charge coupled device spectrometer. The left inset shows the definition of delay times. The right inset depicts the detection scheme and the geometry of the 2D-ES experiment: three laser pulses with wavevectors $\mathbf{k}_1$, $\mathbf{k}_2$, and $\mathbf{k}_3$ create a nonlinear signal ($\mathbf{k}_s = +\mathbf{k}_1 - \mathbf{k}_2 + \mathbf{k}_3$ for $t_1 < 0$; $\mathbf{k}_s = -\mathbf{k}_1 + \mathbf{k}_2 + \mathbf{k}_3$ for $t_1 > 0$), which are spectrally interfered with a local oscillator field (LO) for signal detection and reconstruction in the $\omega_3$-frequency domain.

Downloaded by RENMIN UNIV OF CHINA on October 2, 2009 | http://pubs.acs.org
Publication Date (Web): August 12, 2009 | doi: 10.1021/ar800282e

tronic resonances. To avoid undesired higher-order effects, the excitation beams are attenuated to yield less than 3 nJ of energy in each of the excitation pulses. To avoid nonresonant signals from cell windows, we use a gravity-driven, wire-guided drop jet for circulating the sample solution.[31,32] In all experiments, the three excitation beams are polarized perpendicular to the flow of the jet. According to the projection slice theorem,[20] the absolute phase of the complex signal can be determined by projecting the real part of the 2D spectrum onto an additionally recorded, spectrally resolved pump−probe spectrum.

## Molecular Chromophores of Increasing Complexity

**Electron−Phonon Coupling of an Electronic Two-Level System.** Though modulations of four-wave-mixing signals by vibrational wavepackets are ubiquitous in time-resolved experiments on electronic transitions,[33−35] their signatures in 2D electronic spectra have been addressed only in a handful of theoretical studies.[36−39] This lack of experimental data motivated the investigation of a simple electronic absorber whose third-order spectroscopic signals are dominated by a single, underdamped low-frequency mode.

Figure 2 shows the absorption spectrum of *N*,*N*′-bis(2,6-dimethylphenyl)perylene-3,4,9,10-tetracarboxylicdiimide (PERY) in toluene, which is characterized by the progression of a high-frequency (1400 $cm^{-1}$) mode. Its fundamental $S_1 \leftarrow S_0$ transition can be selected and entirely covered by the spectral bandwidth of our excitation pulses. Under these excitation

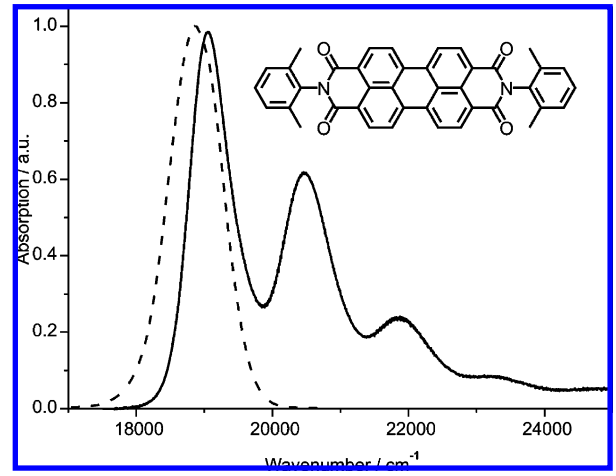


**FIGURE 2.** Absorption spectrum of PERY in toluene (solid line) compared with the spectrum of the excitation pulses (dashed line). The inset shows the chemical structure.

conditions, the third-order signals of PERY exhibit large amplitude modulations, dominated by coupling to a 140 $cm^{-1}$ mode,[35,40] which corresponds to a beating period of 240 fs. Scanning delay $t_2$ in the experiment allows 2D spectra to be recorded at well-separated minima and maxima of the oscillating signal, as illustrated by the sequence of spectra in Figure 3.

For all delays, the positions of the maxima of the absorptive peaks are located below the diagonal ($\omega_3 < |\omega_1|$) and are nearly invariant. However, the ellipticity of the signal peaks is subject to a periodic change. For $t_2$ delays of 200, 450, and 650 fs the absorptive line shapes are of pronounced elliptical shape, with the major axis of the ellipse slanted toward the

Downloaded by RENMIN UNIV OF CHINA on October 2, 2009 | http://pubs.acs.org
Publication Date (Web): August 12, 2009 | doi: 10.1021/ar800282e

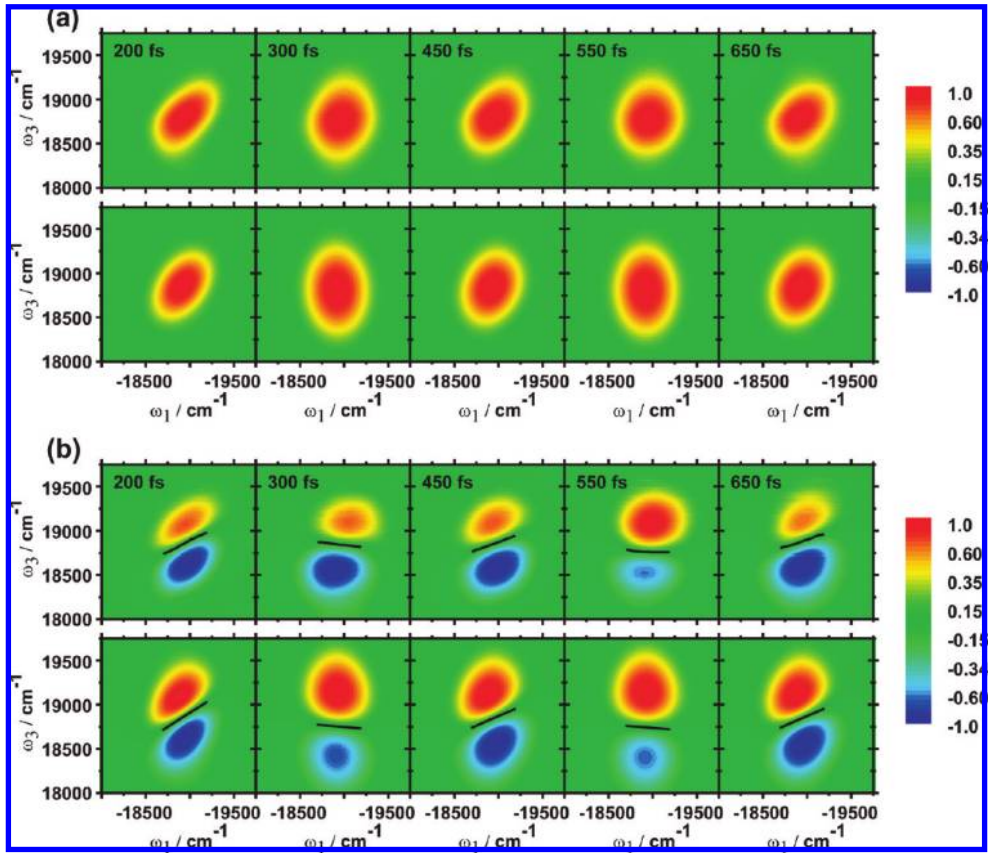


**FIGURE 3.** (a) Absorptive and (b) dispersive 2D spectra of PERY recorded for $t_2$ delays of 200, 300, 450, 550, and 650 fs. The upper rows show experimental data, and the lower ones show simulated data. All spectra are normalized to their respective maximum value, and the color scale is based on a arcsinh-weighting function starting at ±5% of signal intensity.

diagonal. The shape of the 2D peaks for 300 and 500 fs is more circular, and the major axis of the ellipse is almost parallel to the $\omega_3$ axis. Even more pronounced are the changes to the dispersive signal parts, due to two contributions of opposite sign. From Figure 3b, it is obvious that both contributions experience alternating widening and narrowing that is in-phase with the rotation of the major axis of the ellipse in the absorptive signal. The slope of the zero-crossing between the two contributions (drawn as a black solid line in the dispersive parts in Figure 3b) thereby experiences strong changes in its orientation.

Figure 4 summarizes the quantitative analysis of the 2D spectra for an extended $t_2$ sequence. The changes in the ellipticity of the absorptive line shape are quantified by determining diagonal and antidiagonal widths at a peak height of $1/e$.[11] The diagonal widths are larger than the antidiagonal ones and show only a small dependence on the time delay. Contrarily, the antidiagonal peak widths show pronounced oscillations with $t_2$. This opposing behavior is responsible for the strong modulation of the diagonal to antidiagonal peak width ratio (cf. Figure 4a). In turn, as shown in Figure 4b, the angle of the nodal line (with respect to the $\omega_1$ axis) varies over a range of 30° and assumes negative values at points where the absorptive peaks acquire circular shapes.

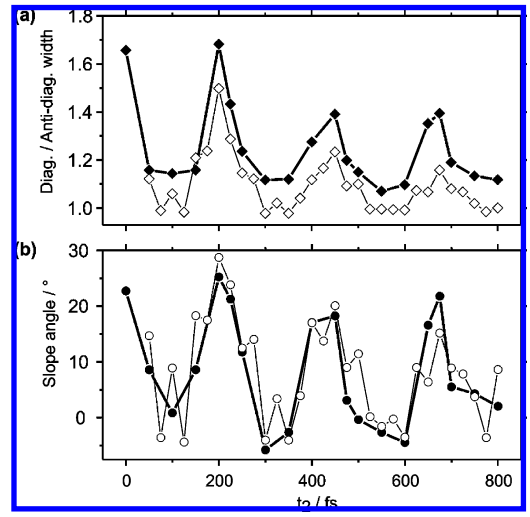


**FIGURE 4.** Analysis of the oscillatory behavior in the 2D spectrum. Both plots share the abscissa of the lower figure: (a) diagonal/antidiagonal peak width ratio of the absorptive signal; (b) angle of the nodal line in the dispersive signal with respect to the $\omega_1$-axis. Filled symbols refer to experimental data, and open symbols refer to calculated data.

Downloaded by RENMIN UNIV OF CHINA on October 2, 2009 | http://pubs.acs.org
Publication Date (Web): August 12, 2009 | doi: 10.1021/ar800282e

To analyze the experimental data, we have performed simulations in the impulsive limit (i.e., for infinitely short pulses), using the second-order cumulant expansion of electron−phonon interactions. We treated PERY as an electronic two-level system that interacts with intramolecular as well as solvent vibrational modes, whose connection to the electronic transition is comprised in the energy gap correlation function (CF). The CF of both the overdamped solvent modes and the underdamped oscillatory modes of PERY are treated within the Brownian oscillator model. The model requires two parameters (reorganization energy, $\lambda$, and correlation time, $\tau_c$) for overdamped modes and three parameters (reorganization energy, $\lambda$, oscillator frequency, $\omega$, and damping, $\gamma$) for the underdamped modes.[41] The third-order nonlinear response functions, which determine the spectroscopic signals, can be expressed in terms of a double integral of the CF, the so-called line-shape function (we refer to ref 21 for further details on the numerically straightforward calculation). As illustrated in Figures 3 and 4, the results of this approach are in excellent agreement with the experiment.

For an intuitive understanding of the periodic spectral changes, we recall that vibrational modes are multilevel structured quantum mechanical systems. Both the ground and excited electronic states of PERY feature levels spaced by vibrational frequency $\omega$, which is much smaller than the bandwidth of the exciting laser pulses. The first two laser pulses thus not only populate vibrational states but also excite coherences between them. During $t_2$ evolution in a 2D experiment, these coherences modulate the signal by a factor $\exp(\pm i\omega t_2)$. In essence, the second-order cumulant approach permits us to include this coherent dynamics together with solvent-induced damping into the CF. By expanding the CF of an underdamped vibrational mode in its Huang−Rhys factor, $\lambda/\omega$, we find the most significant changes in the 2D line shapes to oscillate with the cosine of the population time.[21] Given that $\omega$ is small compared with the electronic energy gap, one can further observe the rephasing and nonrephasing signal parts to oscillate with mutually opposite phase. This behavior is illustrated in Figure 5, where we exemplarily show the (absorptive) rephasing and nonrephasing signal parts for $t_2$ delays of 200 and 300 fs.

**Monomers versus Dimers.** Given that molecules approach each other close enough, the electronic properties of the formed molecular assembly, or aggregate, become size dependent and no longer correspond to the ones of its individual constituents. Rather, molecular aggregates are characterized by the close spatial proximity of coupled molecular transition dipoles and the consequent formation of collective

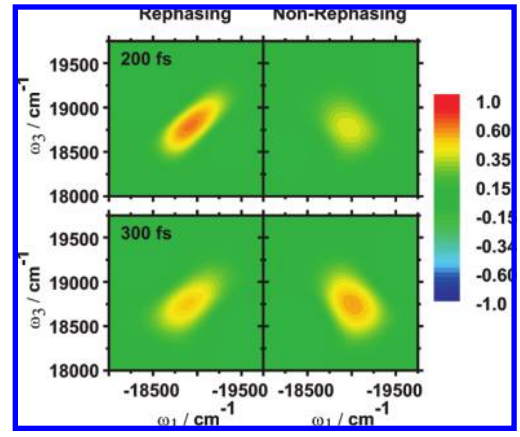


**FIGURE 5.** Rephasing (left) and nonrephasing (right) contributions to the absorptive 2D signal at $t_2$ delays of 200 and 300 fs. The amplitudes of the rephasing and nonrephasing parts are modulated out-of-phase with respect to each other, consequently inducing oscillatory features in the 2D spectrum. The color scale is based on a arcsinh function starting at ±5% signal intensity.

excited states (excitons). Two-dimensional electronic spectroscopy has been introduced as the method of choice for deepening the comprehension of how the interaction strengths and the static and dynamic disorder of the molecular sites are reflected in the optical response of excitonic systems. However, apart from one study on a covalently linked oligophenylene dimer,[9] experiments so far have been focused on rather large complexes, like natural[10−12] or artificial[23,29] light harvesters. This is in some contradiction to the popularity of dimers (as the simplest aggregate prototypes) in theoretical studies of excitonic interactions, and we consider the following results as a step toward closing this gap.

Analyzing suitable molecular systems that offer straightforward access to control the extent of excitation delocalization, one finds a variety of convenient choices from the class of aggregating cyanine dyes. Due to strong dispersion forces associated with the high polarizability of the chromophores, cyanine dyes are well-known to form aggregates in aqueous solutions.[42] The degree of aggregation can be controlled by both solute concentration and the polarity of the solvent. This permits one to study effects of excitation delocalization at the lowest level of aggregation by direct comparison of monomeric and dimeric line shapes in 2D spectra.

According to Frenkel exciton theory, the electronic interaction of aggregating chromophores gives rise to energetically shifted, delocalized exciton states. For the simplest case of a periodic linear arrangement, depending on the mutual orientation of transition dipoles with respect to their centers-of-mass joint, a new dominant absorption band appears, which is either red-shifted (J-aggregates) or blue-shifted (H-aggregates) to the monomer transition. Aggregates of pinacyanol chlo-

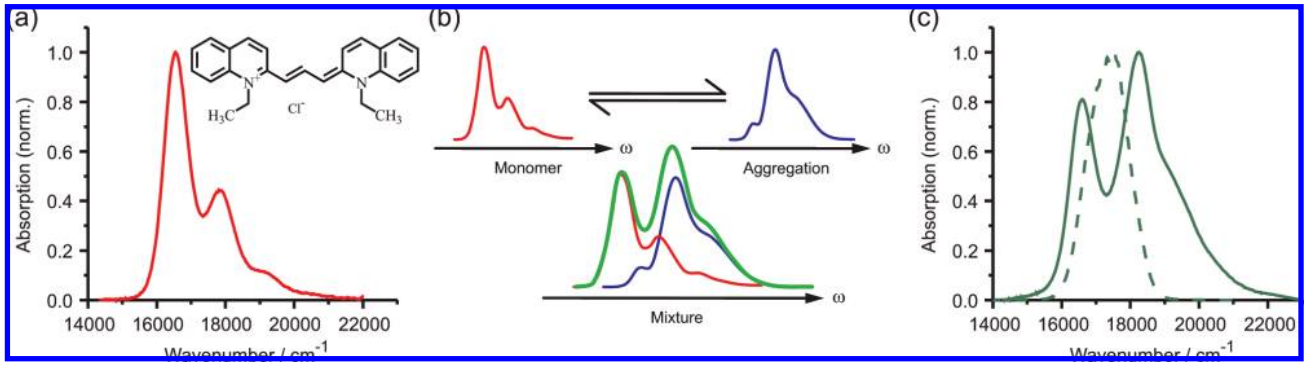


**FIGURE 6.** (a) Linear absorption spectrum of pinacyanol chloride (PIN) in methanol. The chemical structure is shown in the inset. (b) Schematics of new bands appearing upon aggregation of PIN monomers that form dimers and higher aggregates. (c) Absorption spectrum (solid line) of an equilibrated mixture of PIN in a water/methanol solution compared with the laser pulse spectrum (dashed line).

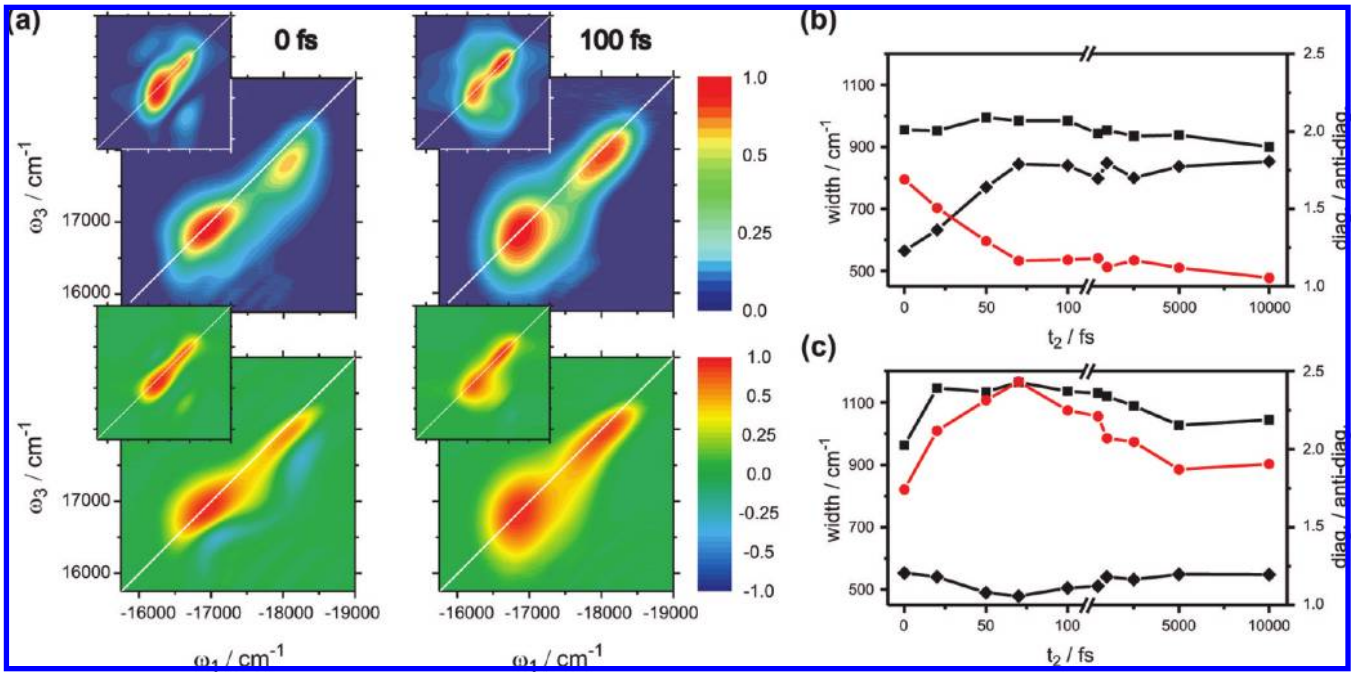


**FIGURE 7.** (a) Amplitude (top) and absorptive (bottom) parts of 2D spectra recorded at $t_2$ delays of 0 and 100 fs. The additional spectra partly overlaid in the upper left corners of each 2D plot display calculated data. The spectra are normalized to their respective maximum value, and the color scale is based on a arcsinh function starting at ±5% of the signal intensity. The line-shape analysis for a full sequence of 2D spectra is shown separately for the momomeric (b) and dimeric (c) peaks. Squares show the evolution of the diagonal peak widths, and diamonds show that of the antidiagonal peak widths; circles show the diagonal to antidiagonal peak width ratio.

Downloaded by RENMIN UNIV OF CHINA on October 2, 2009 | http://pubs.acs.org
Publication Date (Web): August 12, 2009 | doi: 10.1021/ar800282e

ride (PIN, cf. Figure 6a), a prototypical cyanine dye investigated in the present study, belong to the latter type of H-aggregates. Figure 6b schematically explains the spectral pattern of an equilibrated solution of monomers, dimers, and higher aggregates that are present in water−methanol mixtures. According to the common interpretation of the PIN spectrum under conditions of partial aggregation,[42] the three new bands in linear absorption (LA) are assigned to the lower and the upper exciton levels of molecular dimers and an additional blue-shifted band originating from higher aggregates. By tuning the solvent polarity, one can adjust the concentrations of the different absorbers for a double-peaked LA spectrum with what we refer to as a monomeric and a dimeric absorption maximum in the following (cf. Figure 6c).

As illustrated in Figure 7a, the bandwidth of our excitation pulses is broad enough to recover both peaks in the amplitude and absorptive part of the 2D spectra. At $t_2 = 0$ fs, the two features exhibit a pronounced elliptical shape with the major axes of the ellipses slanted toward the diagonal with slightly different orientations. As revealed by a quantitative line shape analysis of a $t_2$ sequence up to 10 ps (cf. Figure 7b,c), the similarity of the two peaks, despite remarkably similar diagonal and antidiagonal widths in the ($t_2 = 0$) correlation spectrum, vanishes on a sub-100 fs time scale. While the

antidiagonal width of the monomer steeply rises within the first 50 fs, its diagonal width remains essentially unchanged (Figure 7b). The diagonal to antidiagonal peak width ratio thus quickly decays to a value close to unity. This quick loss of memory is typical for molecular absorbers in the condensed phase.[34,43] In contrast, Figure 7c demonstrates the evolution of the peak width ratio for the dimer peak to be mainly determined by changes in the diagonal width and to level off at roughly twice the value as that for the monomer.

As is well-known, the delocalization degree of an electronic excitation affects the contributions from both static and dynamic disorder to the spectral line shape. As for static disorder, the effect refers to the reduction of spectral inhomogeneity as a result of statistic sampling over independent sites. In the present case, the increase in diagonal width for the dimer resembles a broad distribution of monomer distances and orientations, which are static on the time scale of the experiment (inhomogeneous broadening). On the other hand, the exchange narrowing of dynamical fluctuations (homogeneous broadening) acts toward a reduction of the antidiagonal width in the 2D line shape of the dimer. Qualitatively, our observations indicate the solvent-induced transition energy fluctuations of the electronically interacting monomers to be independent (uncorrelated) of each other. The actual extent of the effect depends on the particular form of the correlation function assumed for the monomeric sites. Because a more elaborate discussion of simulations is beyond the scope here, we only note that a simple transfer of parameters extracted from the monomeric line shape cannot fully account for the observed dynamics of the dimer. Rather, the experimentally observed antidiagonal narrowing is higher than one would predict from a Frenkel exciton model, and distinct system–bath coupling characteristics have to be assumed for reproducing the experiment (see insets in Figure 7a). The origin of this trend is unveiled by a quantum chemical analysis of the dimer's electronic structure.[22]

**Exciton Dynamics in a Molecular Nanotube.** As illustrated above for the simplest possible case of a molecular homodimer, the fluctuational dynamics of delocalized excitations significantly differs from the one of noninteracting chromophores. This effect of exchange narrowing becomes increasingly significant when the number of molecules sharing an excitonic state increases. The effectiveness of photosynthetic light-harvesting complexes, in fact, relies on the delocalization and the directed transfer of excited states on large, ordered arrangements of molecular absorbers. Accordingly, the realization of long-range molecular order, coherent excitation delocalization, and defined relaxation pathways

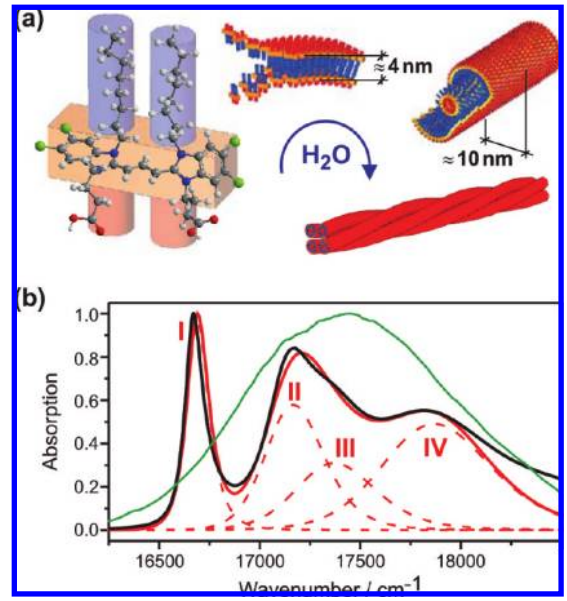


**FIGURE 8.** (a) Scheme of the self-assembling mechanism of $C_8O_3$. The $\pi$-electron system responsible for absorption is displayed as the orange middle part, the hydrophilic side chains as red tubes, and the hydrophobic side chains as blue tubes. (b) The experimental linear absorption spectrum of $C_8O_3$ (black line), and its reconstruction with four electronic oscillators (dashed red lines show individual contributions; the sum is shown as a solid red line). The laser pulse spectrum is shown as solid green line for comparison.

are central issues in the design of bioinspired devices with engineered energy flows. Though self-assembled cylindrical molecular aggregates have emerged as excellent candidates to meet this criteria, the how and why of energy transport in tubular aggregates is not fully understood. In this final section, we present the emerging picture of the spatiotemporal exciton relaxation pathways as derived from 2D-ES experiments.

The simultaneous linking of both hydrophobic and hydrophilic substituents to aggregate forming dyes is a novel ansatz in the development of artificial light harvesters and relies on combining the self-organization tendency of organic surfactants with selected, highly polarizable molecular absorbers. The basic scheme for the self-assembling mechanism of $C_8O_3$,[44] the particular system chosen for this contribution, shown in Figure 8a, is thereby common for a broad range of molecular nanotubes. In aqueous solution, the hydrophobic interactions of aliphatic side chains facilitate the formation of bilayers, which self-assemble into cylindrical double-walled structures with typical diameters of roughly 10 nm.[45] For $C_8O_3$, the double-walled strands further build up helices in which up to five tubules twist around each other forming a chiral superstructure. The possible application of these systems as building blocks for artificial light-harvesting devic-

Downloaded by RENMIN UNIV OF CHINA on October 2, 2009 | http://pubs.acs.org
Publication Date (Web): August 12, 2009 | doi: 10.1021/ar800282e

Downloaded by RENMIN UNIV OF CHINA on October 2, 2009 | http://pubs.acs.org
Publication Date (Web): August 12, 2009 | doi: 10.1021/ar800282e

es[46] or nanometer-scale wires for energy transport[47] renders the characterization of energy flow pathways and time scales a topic of high interest.

In the infinite limit, the linear absorption of a single-walled cylindrical aggregate is split by its symmetry into two transitions oriented parallel and perpendicular to the cylinder axis.[48] As shown in Figure 8b, the linear absorption spectrum of $C_8O_3$ in water exhibits four excitonic bands, three of them (termed bands I, II, and IV) polarized preferentially parallel and one polarized mainly perpendicular to the cylinder axis (band III, Figure 8b). In a widely accepted picture, bands I and II reflect longitudinally polarized transitions that are essentially located on the inner and the outer cylinder, respectively.[49] The blue shift of band II with respect to band I, in combination with the larger diameter of the outer tube, is assumed to merge both of the two perpendicular transitions associated with the two walls into one band (band III). Band IV presumably originates from electronic excitations shared by several close-lying tubules in the helical architecture, similar to the collective excitations in chlorosomal stacks.[50] This multiband structure of linear absorption can be well reconstructed by four effective electronic oscillators, as shown by the red line in Figure 8b.

The sequence of 2D-ES spectra in Figure 9 reveals the pathways and time scales of exciton motion that are hidden in linear absorption. Comparing the diagonal ($|\omega_1| = \omega_3$) amplitude maxima in the 2D correlation spectrum ($t_2 = 0$ fs, top panel of Figure 9a), we can identify the spectral positions of bands I−IV, as defined in Figure 8b. The instantaneous observation of off-diagonal features at all of the possible band crossings in the $|\omega_1| > \omega_3$ triangular signal part indicates that all bands are coupled among each other. The most prominent off-diagonal intensities at zero delay stem from strong correlations between bands I and III (giving rise to an isolated cross-peak), as well as from couplings between bands II and IV. The off-diagonal intensities are thereby stretched along $\omega_1$, reflecting an increasingly dense distribution of exciton states that share a common ground state.

Upon examination of the absorptive part of the 2D signal (Figure 9c), we can dissect the different pathways that interfere to form the observed 2D spectral pattern. Excitonic intermolecular couplings reshape an aggregate's electronic structure to a manifold of single- and double-excited states, referred to as the one- and the two-exciton manifold, respectively. As a consequence of the repulsive interaction between excitons, transitions between successively higher excitonic manifolds are blue-shifted with respect to each other. Positive contributions to the absorptive 2D signal can thus be assigned to ground-state bleaching (GSB) and stimulated emission contributions from one-exciton states (SE), negative contributions, in turn, arise from excited-state absorption (ESA) into the two-exciton manifold.[41] For the diagonal peaks of bands I, II, and III, we observe the positive and negative contributions to be of equal strength, whereas band IV shows a weak positive feature only. On the other hand, on early time scales, the off-diagonal features in $|\omega_1| > \omega_3$ are dominated by positive contributions.

By recording a sequence of 2D spectra for ($t_2$) delays up to 500 fs, we can directly trace the excitation transfer pathways and categorize the relaxational dynamics into three regimes (cf. Figure 9). Within the first 50 fs, the onset of energetic downhill transfer leads to the disappearance of the weak signal of band IV, accompanied by a relative increase of all off-diagonal features in $|\omega_1| > \omega_3$. Population transfer, as controlled by the electronic coupling pattern, causes the transformation of the off-diagonal signals into streak-like shapes, thus mapping out the most efficient relaxation channels. After 200 fs, the 2D spectrum is mainly governed by relaxation from states in the vicinity of band III. This causes streaking of band II along $\omega_1$ resolving the coupling between bands III and II originally hidden under the intense diagonal peak. At $t_2 =$ 500 fs, we mainly observe relaxation from band II into band I, a process that completes the exciton funneling into the lowest accessible state.

In contrast to the assessable number of coupled pigments in most of the natural antennas that are in the focus of experimental studies, molecular nanotubes are huge with respect to their building blocks. The sheer number of molecules building up the tubular structure is an obstacle in any theoretical approach that aims to account for individual site properties (like site orientation or static site disorder). Recalling that the calculation of the third-order nonlinear response of $N$ excitonically coupled two-level systems requires explicit information of the $N$ single- and the $N(N-1)/2$ double-excited eigenstates,[41] a microscopic model is precluded by current computational limits. In order to simulate the experimental data with reasonable effort, we thus resort to an effective level scheme of single- and double-excited states. Briefly, we start in the basis of products of single-exciton eigenstate space excitations,[51] which applies for an arbitrary molecular complex. Each of the four exciton bands is treated as an electronic three-level system coupled to an overdamped Brownian oscillator.[41] The one- and two-exciton transitions associated with each of the bands I−IV are modeled by adjusting the positions and intensities for best match with the linear spectrum, as well as the positive and negative contributions to the diag-

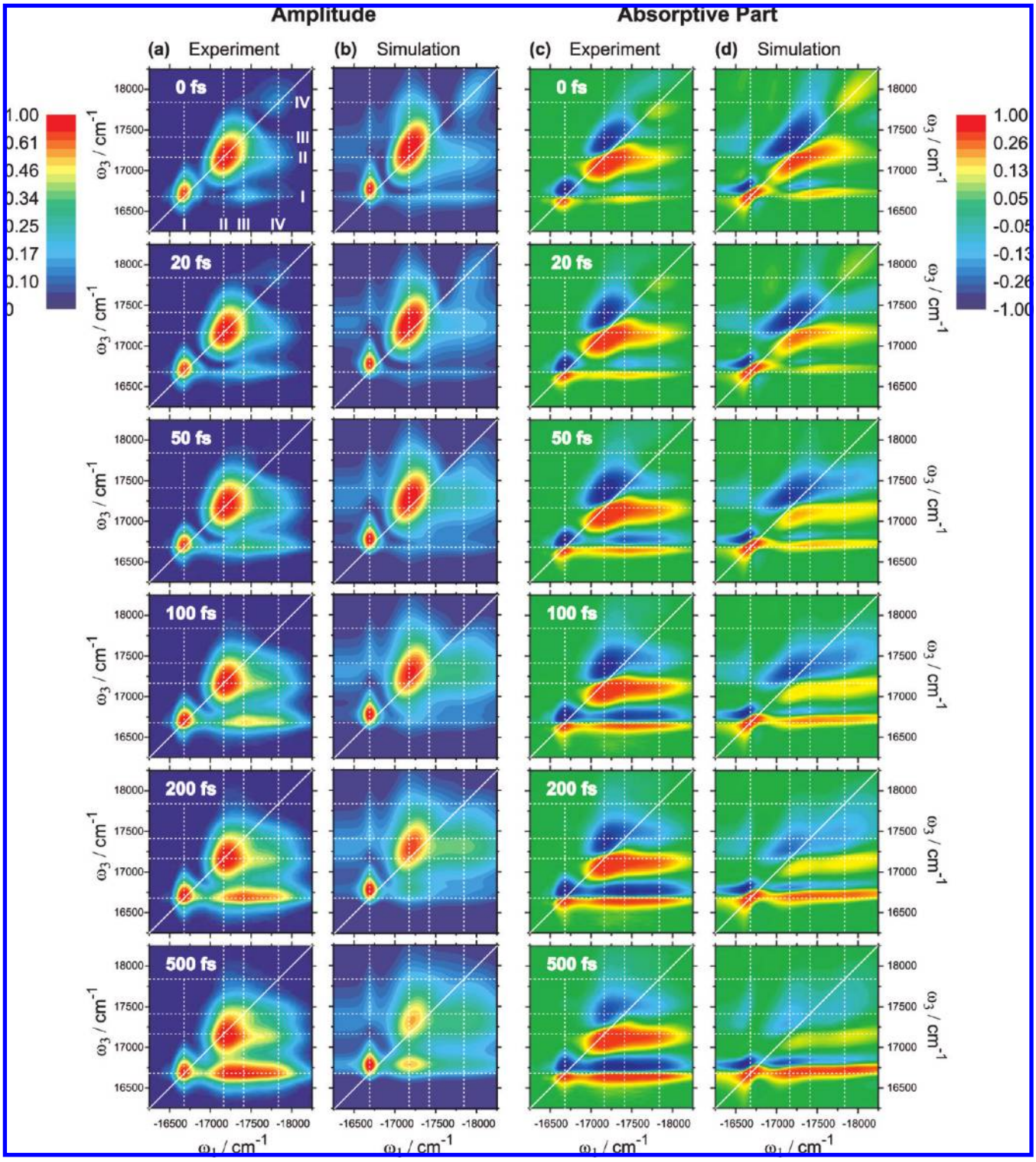


**FIGURE 9.** (a) Amplitude and (b) absorptive part representation of 2D spectra of $C_8O_3$ for $t_2$ delays of 0, 20, 50, 100, 200, and 500 fs (from top to bottom). Panels on the left show experimental data, and those on the right show simulated data; all spectra are normalized to their respective maximum absolute value. White dotted lines indicate the peak positions in linear absorption.

onal peaks of the absorptive part. To model off-diagonal signal intensities, six double-excited states are adjusted as follows. For a particular double-excited state, an energetic offset from the sum of the two single-excitation energies involved is included, which accommodates exciton-repelling interactions and thereby induces a cross-peak. Interband excitation transfer rates are fitted by simulating the dissipative quantum dynamics using a Pauli master equation. In the glo-

Downloaded by RENMIN UNIV OF CHINA on October 2, 2009 | http://pubs.acs.org
Publication Date (Web): August 12, 2009 | doi: 10.1021/ar800282e

bal fitting procedure, we allow for iterative adjustment of population transfer rates among all of the bands I−IV.

As shown in Figure 9b,d, the essential dynamics in diagonal and off-diagonal signal contributions can be captured satisfactorily with this procedure. The key findings of our approach can be summarized as the exciton lifetimes for bands IV−II, for which we find 50 fs (band IV), 174 fs (band III), and 403 fs (band II) (the experimentally observed population decay from band I due to fluorescence is not accounted for in our simulations). Considering that the excitation energy transfer rates vary over roughly an order of magnitude, we conclude that cascading energy transfer pathways play a substantial role in the downhill energy transfer of high-energy excitons into the lowest energy band I, with intermediate states in the vicinity of band II.

Overall, the combination of the outlined simulation method with experimental results from 2D-ES allows us to quantify the coupling and relaxation pattern of large excitonic systems that become quickly untractable with microscopic approaches. To close, we point out that an effective level scheme explains the band-to-band coupling and its origin by double-quantum combination transitions. From this point-of-view, the excitation fields can act on two different single-excited states ($|e_1\rangle$ and $|e_2\rangle$), which can be seen as a double-excited combination transition $|e_1e_2\rangle$. The contributions of these combination transitions exactly cancel in the case of noninteracting single-excited states, that is, if the transition moments are kept (i.e., $\mu_{ge_2}$ connects $|e_1\rangle \rightarrow |e_1e_2\rangle$ and $\mu_{ge_1}$ connects $|e_2\rangle \rightarrow |e_1e_2\rangle$) and the energy of the double-excited (combination) state matches the sum of the two states involved. By shifting the combination transition energy, one can eliminate this cancelation and induce a cross-peak. This corresponds to exciton-repelling interactions and provides a sensitive test for extracting the coupling pattern between excitonic bands from the experiment.

Downloaded by RENMIN UNIV OF CHINA on October 2, 2009 | http://pubs.acs.org
Publication Date (Web): August 12, 2009 | doi: 10.1021/ar800282e

## Outlook

By performing 2D-ES experiments on molecular systems of varying complexity, we illustrate the huge potential of the method in simply visualizing the physics behind the complex signal shapes provided by other third-order techniques. Although 2D-ES is far from being a "turn-key" method, one can expect, as with multidimensional NMR and 2D-IR, that over the next years progress in the experimental field and possible commercialization of the instrumentation will lead to proliferation of the method and will make 2D-ES accessible to a much broader scientific audience. Similar to the advancement of 2D-IR to 2D-ES, it is only natural to expect the development of the method toward even shorter wavelengths for covering, for example, the absorption region of DNA. Extensions of the method for correlation of single and double quantum coherences, as already illustrated in first experiments,[15] bear exciting experimental access to many-body correlations.

*This work was supported by the Austrian Science Foundation (FWF) within the Projects F016-18 (ADLIS) and P18233. A.N. and J.S. acknowledge partial funding by the Austrian Academy of Sciences (DOC-fFORTE and DOC). T.M. acknowledges the support by the Czech Science Foundation through Grant GACR 202/07/P278 and by the Ministry of Education, Youth, and Sports of the Czech Republic through Research Plan MSM0021620835.*

### BIOGRAPHICAL INFORMATION

**Franz Milota** (University of Vienna), whose research interests have covered various aspects of ultrafast instrumentation, shares the major contribution in the experimental implementation of the method.

**Jaroslaw Sperling** (University of Vienna) enjoys connecting strategies in experiment and theory for addressing open questions in the molecular physics of excitonic systems.

**Alexandra Nemeth** (University of Vienna) currently works on extending the method for investigation of double-quantum coherences and its combination with pulse-shaping techniques.

**Tomáš Mančal**'s (Charles University, Prague) main interests lie in the theory of open quantum systems, as well as charge and energy transfer phenomena, mostly in connection with biological systems.

**Harald F. Kauffmann** (Ph.D., Chemistry 1971, University of Vienna) leads the Ultrafast Dynamics Group at the University of Vienna/Vienna University of Technology, which is concerned with experimental methods of nonlinear femtosecond spectroscopy to study optical coherence in complex molecules and exciton dynamics in molecular many-body systems.

### FOOTNOTES

* To whom correspondence should be addressed. E-mail: harald.f.kauffmann@univie.ac.at.
§ Current address: Newport-Spectra Physics GmbH, 64291 Darmstadt, Germany.

### REFERENCES

1 Wüthrich, K. *NMR of Proteins and Nucleic Acids*; Wiley: New York, 1986.
2 Ernst, R. R.; Bodenhausen, G.; Wokaun, A. *Principles of Nuclear Magnetic Resonance in One and Two Dimensions*; Clarendon Press: Oxford, U.K., 1987.
3 Tanimura, Y.; Mukamel, S. Two-dimensional femtosecond vibrational spectroscopy of liquids. *J. Chem. Phys.* **1993**, *99*, 9496–9511.
4 Tokmakoff, A.; Fayer, M. D. Infrared photon echo experiments: Exploring vibrational dynamics in liquids and glasses. *Acc. Chem. Res.* **1995**, *28*, 437–445.
5 Hamm, P.; Lim, M.; Hochstrasser, R. M. Structure of the amide I band of peptides measured by femtosecond nonlinear-infrared spectroscopy. *J. Phys. Chem. B* **1998**, *102*, 6123–6138.
6 Mukamel, S. Multidimensional femtosecond correlation spectroscopy of electronic and vibrational excitations. *Annu. Rev. Phys. Chem.* **2000**, *51*, 691–729.

7 Hybl, J. D.; Albrecht, A. W.; Faeder, S. M. G.; Jonas, D. M. Two-dimensional electronic spectroscopy. *Chem. Phys. Lett.* **1998**, *297*, 307–313.

8 Hybl, J. D.; Ferro, A. A.; Jonas, D. M. Two-dimensional Fourier transform electronic spectroscopy. *J. Chem. Phys.* **2001**, *115*, 6606–6622.

9 Moran, A. M.; Maddox, J. B.; Hong, J. W.; Kim, J.; Nome, R. A.; Bazan, G. C.; Mukamel, S.; Scherer, N. F. Optical coherence and theoretical study of the excitation dynamics of a highly symmetric cyclophane-linked oligophenylenevinylene dimer. *J. Chem. Phys.* **2006**, *124*, 194904.

10 Brixner, T.; Mančal, T.; Stiopkin, I. V.; Fleming, G. R. Phase-stabilized two-dimensional electronic spectroscopy. *J. Chem. Phys.* **2004**, *121*, 4221–4236.

11 Engel, G. S.; Calhoun, T. R.; Read, E. L.; Ahn, T. K.; Mančal, T.; Cheng, Y. C.; Blankenship, R. E.; Fleming, G. R. Evidence for wavelike energy transfer through quantum coherence in photosynthetic systems. *Nature* **2007**, *446*, 782–786.

12 Read, E. L.; Schlau-Cohen, G. S.; Engel, G. S.; Wen, J.; Blankenship, R. E.; Fleming, G. R. Visualization of excitonic structure in the Fenna-Matthews-Olson photosynthetic complex by polarization dependent two-dimensional electronic spectroscopy. *Biophys. J.* **2008**, *95*, 847–856.

13 Zhang, T.; Borca, C. N.; Li, X.; Cundiff, S. T. Optical two-dimensional Fourier transform spectroscopy with active interferometric stabilization. *Opt. Express* **2005**, *13*, 7432–7441.

14 Vaughan, J. C.; Hornung, T.; Stone, K. W.; Nelson, K. A. Coherently controlled ultrafast four-wave mixing spectroscopy. *J. Phys. Chem. A* **2007**, *111*, 4873–4883.

15 Gundogdu, K.; Stone, K. W.; Turner, D. B.; Nelson, K. A. Multidimensional coherent spectroscopy made easy. *Chem. Phys.* **2007**, *341*, 89–94.

16 Tian, P.; Keusters, D.; Suzaki, Y.; Warren, W. S. Femtosecond phase-coherent two-dimensional spectroscopy. *Science* **2003**, *300*, 1553–1555.

17 Grumstrup, E. M.; Shim, S.-H.; Montgomery, M. A.; Damrauer, N. H.; Zanni, M. T. Facile collection of two-dimensional electronic spectra using femtosecond pulse-shaping technology. *Opt. Express* **2007**, *15*, 16681–16689.

18 Lepetit, L.; Joffre, M. Two-dimensional nonlinear optics using Fourier-transform spectral interferometry. *Opt. Lett.* **1996**, *21*, 564–566.

19 Lepetit, L.; Chériaux, G.; Joffre, M. Linear techniques of phase measurements by femtosecond spactral interferometry for application in spectroscopy. *J. Opt. Soc. Am. B* **1995**, *12*, 2467–2474.

20 Jonas, D. M. Two-dimensional femtosecond spectroscopy. *Annu. Rev. Phys. Chem.* **2003**, *54*, 425–463.

21 Nemeth, A.; Milota, F.; Mančal, T.; Lukeš, V.; Kauffmann, H. F.; Sperling, J. Vibronic modulation of lineshapes in two-dimensional electronic spectra. *Chem. Phys. Lett.* **2008**, *459*, 94–99.

22 Nemeth, A.; Lukeš, V.; Sperling, J.; Milota, F.; Kauffmann, H. F.; Mančal, T. 2D electronic spectra of an aggregating dye: Simultaneous measurement of monomeric and dimeric lineshapes. *Phys. Chem. Chem. Phys.* **2009**, *11*, 5986–5997.

23 Nemeth, A.; Milota, F.; Sperling, J.; Abramavicius, D.; Mukamel, S.; Kauffmann, H. F. Tracing exciton dynamics in molecular nanotubes with 2D electronic spectroscopy. *Chem. Phys. Lett.* **2009**, *469*, 130–134.

24 Milota, F.; Sperling, J.; Nemeth, A.; Abramavicius, D.; Mukamel, S.; Kauffmann, H. F. Excitonic couplings and inter-band energy transfer in a double-wall molecular aggregate imaged by coherent 2D electronic spectroscopy. *J. Chem. Phys.* **2009**,*131*, 054510.

25 Piel, J.; Riedle, E.; Gundlach, L.; Ernstorfer, R.; Eichberger, R. Sub-20 fs visible pulses with 750 nJ energy from a 100-kHz noncollinear optical parametric amplifier. *Opt. Lett.* **2006**, *31*, 1289–1291.

26 Baum, P.; Breuer, M.; Riedle, E.; Steinmeyer, G. Brewster-angled chirped mirrors for broadband pulse compression without dispersion oscillations. *Opt. Lett.* **2006**, *31*, 2220–2222.

27 Baum, P.; Lochbrunner, S.; Riedle, E. Zero-additional-phase SPIDER: Full characterization of visible and sub-20-fs ultraviolet pulses. *Opt. Lett.* **2004**, *29*, 210–212.

28 Cowan, M. L.; Ogilvie, J. P.; Miller, R. J. D. Two-dimensional spectroscopy using diffractive optics based phased-locked photon-echoes. *Chem. Phys. Lett.* **2004**, *386*, 184–189.

29 Milota, F.; Sperling, J.; Nemeth, A.; Kauffmann, H. F. Two-dimensional electronic photon echoes of a double band J-aggregate: Quantum oscillatory motion versus exciton relaxation. *Chem. Phys.* **2009**, *357*, 45–53.

30 Khalil, M.; Demirdöven, N.; Tokmakoff, A. Obtaining absorptive line shapes in two-dimensional infrared vibrational correlation spectra. *Phys. Rev. Lett.* **2003**, *90*, 047401.

31 Tauber, M. J.; Mathies, R. A.; Chen, X.; Bradforth, S. E. Flowing liquid sample jet for resonant Raman and ultrafst optical spectroscopy. *Rev. Sci. Instrum.* **2003**, *74*, 4958–4960.

32 Laimgruber, S.; Schachenmayr, H.; Schmidt, B.; Zinth, W.; Gilch, P. A femtosecond stimulated Raman spectrograph for the near ultraviolet. *Appl. Phys. B: Lasers Opt.* **2006**, *85*, 557–564.

33 Ohta, K.; Larsen, D. S.; Yang, M.; Fleming, G. R. Influence of intramolecular vibrations in third-order, time-domain resonant spectroscopies. II. Numerical calculations. *J. Chem. Phys.* **2001**, *114*, 8020–8039.

34 de Boeij, W. P.; Pshenichnikov, M. S.; Wiersma, D. A. System−bath correlation function probed by conventional and time-gated stimulated photon echo. *J. Phys. Chem.* **1996**, *100*, 11806–11823.

35 Larsen, D. S.; Ohta, K.; Xu, Q.-H.; Cyrier, M.; Fleming, G. R. Influence of intramolecular vibrations in third-order, time-domain resonant spectroscopies. I. Experiments. *J. Chem. Phys.* **2001**, *114*, 8008–8019.

36 Gallagher Faeder, S. M.; Jonas, D. M. Two-dimensional electronic correlation and relaxation spectra: Theory and model calculations. *J. Phys. Chem. A* **1999**, *103*, 10489–10505.

37 Egorova, D.; Gelin, M. F.; Domcke, W. Analysis of vibrational coherences in homodyne and two-dimensional heterodyne photon-echo spectra of Nile Blue. *Chem. Phys.* **2007**, *341*, 113–122.

38 Egorova, D.; Gelin, M. F.; Domcke, W. Analysis of cross peaks in two-dimensional electronic photon-echo spectroscopy for simple models with vibrations and dissipation. *J. Chem. Phys.* **2007**, *126*, 074314.

39 Egorova, D. Detection of electronic and vibrational coherences in molecular systems by 2D electronic photon echo spectroscopy. *Chem. Phys.* **2008**, *347*, 166–176.

40 Larsen, D. S.; Ohta, K.; Fleming, G. R. Three pulse photon echo studies of nondipolar solvation: Comparison with a viscoelastic model. *J. Chem. Phys.* **1999**, *111*, 8970–8979.

41 Mukamel, S. *Principles of Nonlinear Optical Spectroscopy*; Oxford University Press: New York, 1995.

42 West, W.; Pearce, S. The dimeric state of cyanine dyes. *J. Phys. Chem.* **1965**, *69*, 1894–1903.

43 Cho, M.; Yu, J.-Y.; Joo, T.; Nagasawa, Y.; Passino, S. A.; Fleming, G. R. The integrated photon echo and solvation dynamics. *J. Phys. Chem.* **1996**, *100*, 11944–11953.

44 $C_8O_3$ = 5,5′,6,6′-tetrachloro-1,1′-dioctyl-3,3′-di-(3-carboxypropyl)-benzimidacarbocyanine.

45 von Berlepsch, H.; Böttcher, C.; Ouart, A.; Burger, C.; Dähne, S.; Kirstein, S. Supramolecular structures of J-aggregates of carbocyanine dyes in solution. *J. Phys. Chem. B* **2000**, *104*, 5255–5262.

46 Balaban, T. S. Tailoring porphyrins and chlorins for self-assembly in biometic artificial antenna systems. *Acc. Chem. Res.* **2005**, *38*, 612–623.

47 Takazawa, K.; Kitahama, Y.; Kimura, Y.; Kido, G. Optical waveguide self-assembled from organic dye molecules in solution. *Nano Lett.* **2005**, *5*, 1293–1296.

48 Didraga, K.; Klugkist, J. A.; Knoester, J. Optical properties of helical cylindrical molecular aggregates: The homogeneous limit. *J. Phys. Chem. B* **2002**, *106*, 11474–11486.

49 von Berlepsch, H.; Kirstein, S.; Hania, R.; Didraga, C.; PugŽlys, A.; Böttcher, C. Stabilitation of individual tubular J-aggregates by poly(vinyl alcohol). *J. Phys. Chem. B* **2003**, *107*, 14176–14184.

50 Prokhorenko, V. I.; Steensgaard, D. B.; Holzwarth, A. R. Exciton theory for supramolecular chlorosomal aggregates: 1. aggregate size dependence of the linear spectra. *Biophys. J.* **2003**, *85*, 3173–3186.

51 Abramavicius, D.; Voronine, D. V.; Mukamel, S. Unravelling coherent dynamics and energy dissipation in photosynthetic complexes by 2D spectroscopy. *Biophys. J.* **2008**, *94*, 3613.


Downloaded by RENMIN UNIV OF CHINA on October 2, 2009 | http://pubs.acs.org
Publication Date (Web): August 12, 2009 | doi: 10.1021/ar800282e